



Unstable evolution of railway slope under the rainfall-vibration joint action

Haoyu DONG, Jiading WANG, Dengfei ZHANG, Lin LI, Yuanjun XU

View online: <https://doi.org/10.1007/s11629-023-8352-7>

Articles you may be interested in

[Centrifuge and numerical modeling of h-type anti-slide pile reinforced soil-rock mixture slope](#)

Journal of Mountain Science. 2023, 20(5): 1441 <https://doi.org/10.1007/s11629-022-7446-y>

[Flow-slide characteristics and failure mechanism of shallow landslides in granite residual soil under heavy rainfall](#)

Journal of Mountain Science. 2022, 19(6): 1541 <https://doi.org/10.1007/s11629-022-7315-8>

[Cumulative damage effect on debris slopes under frequent microseisms](#)

Journal of Mountain Science. 2022, 19(3): 781 <https://doi.org/10.1007/s11629-020-6419-2>

[Mechanism of colluvial landslide induction by rainfall and slope construction: A case study](#)


Journal of Mountain Science. 2021, 18(4): 1013 <https://doi.org/10.1007/s11629-020-6048-9>



[Stability characteristics of shallow landslide triggered by rainfall](#)



Journal of Mountain Science. 2019, 16(9): 2171 <https://doi.org/10.1007/s11629-019-5523-7>


Original Article


Unstable evolution of railway slope under the rainfall-vibration joint action

DONG Haoyu  <https://orcid.org/0000-0002-7986-6186>; e-mail: donghy3510336989@163.com

WANG Jiading*  <https://orcid.org/0000-0001-9087-5035>;  e-mail: wangjd@nwu.edu.cn

ZHANG Dengfei*  <https://orcid.org/0000-0001-7231-3792>;  e-mail: dfzhang87@nwu.edu.cn

LI Lin  <https://orcid.org/0009-0003-1626-6532>; e-mail: linlinli2000@126.com

XU Yuanjun  <https://orcid.org/0000-0002-4613-6582>; e-mail: graceyxu@163.com

*Corresponding author

State Key Laboratory of Continental Dynamics, Department of Geology, Northwest University, Xi'an 710069, China

Citation: Dong HY, Wang JD, Zhang DF, et al. (2024) Unstable evolution of railway slope under the rainfall-vibration joint action. *Journal of Mountain Science* 21(4). <https://doi.org/10.1007/s11629-023-8352-7>

© Science Press, Institute of Mountain Hazards and Environment, CAS and Springer-Verlag GmbH Germany, part of Springer Nature 2024

Abstract: Understanding the unstable evolution of railway slopes is the premise for preventing slope failure and ensuring the safe operation of trains. However, as two major factors affecting the stability of railway slopes, few scholars have explored the unstable evolution of railway slopes under the joint action of rainfall-vibration. Based on the model test of sandy soil slope, the unstable evolution process of slope under locomotive vibration, rainfall, and rainfall-vibration joint action conditions was simulated in this paper. By comparing and analyzing the variation trends of soil pressure and water content of slope under these conditions, the change laws of pore pressure under the influence of vibration and rainfall were explored. The main control factors affecting the stability of slope structure under the joint action conditions were further defined. Combined with the slope failure phenomena under these three conditions, the causes of slope instability resulting from each leading factor were clarified. Finally, according to the above conclusions, the unstable evolution of the slope under the rainfall-vibration joint action was determined. The test results show that the unstable evolution process of sandy soil slope, under the rainfall-vibration joint action, can be

divided into: rainfall erosion cracking, vibration promotion penetrating, and slope instability sliding three stages. In the process of slope unstable evolution, rainfall and vibration play the roles of inducing and promoting slide respectively. In addition, the deep cracks, which are the premise for the formation of the sliding surface, and the violent irregular fluctuation of soil pressure, which reflects the near penetration of the sliding surface, constitute the instability characteristics of the railway slope together. This paper reveals the unstable evolution of sandy soil slopes under the joint action of rainfall-vibration, hoping to provide the theoretical basis for the early warning and prevention technology of railway slopes.

Keywords: Rainfall vibration joint action; Small scale model tests; Unstable evolution process; Unstable characteristics; Inducing sliding and promoting sliding

1 Introduction

As we all know, the rapid development of China's railways in recent years has greatly relieved the transportation pressure in mountainous areas.

Received: 21-Sep-2023

1st Revision: 24-Nov-2023

2nd Revision: 29-Jan-2024

Accepted: 20-Feb-2024

However, in the construction and operation of the railway, some new geological disasters emerge immediately. Such as the top has tunnel deformation and collapse, the bottom has track vibration sink and vibration down, slope sliding and squeezing on the left side, and rainfall scouring and dragging on the right side. Among the threats, the failure problem of slope caused by locomotive vibration and rainfall is the most serious. For example, the railway section from Zhanghu Town to Shuangkeng of China's Waifu line is interrupted by a landslide, the railway section in Chipping Sodbury, South Gloucestershire, UK is paralyzed by a landslide, and the railway section from Kallar to Hillgrove, India is buried by a landslide (Fig. 1). No matter it is a landslide squeezing on the railway, resulting in deformation and damage to the tracks, or a landslide sliding above the railway, resulting in the burying and accumulation of the tracks. For the railway system, the standard of deformation requires a millimeter level. The disasters are the chain of major disasters. The consequences are an unpredictable huge catastrophe.

There are many factors affecting slope stability and the most common one is rainfall. Two serious rock landslides occurred in Emei County, Sichuan Province in China. Ma et al. (2018) found that continuous rainfall would lead to tuff dissolution and reduce the effective stress of rock slopes, thus triggering rock landslides. Also in Sichuan, He et al. (2019) conducted a detailed investigation on a catastrophic landslide in 2017, and found that rainfall would further reduce the strength of weathered basalt and the shear strength of slope, thus triggering rock landslide. In summary, the decrease of surface strength parameters of rock and soil is the main reason of rain-induced rock landslide,

which is completely consistent with the conclusions of Zhou et al. (2021) In fact, not only rock landslide, the safety factor of any slope will continue to decrease as long as the rainfall continues for a long enough time. When the duration exceeds about 576 hours, there is the possibility of inducing landslide (Hou et al. 2021 and Li et al. 2022). Compared with rock slope, unsaturated soil slope with negative pore water pressure (suction) is more susceptible to rainfall. Wu et al. (2017) and Kim et al. (2021), show that the significant reduction of negative pore water pressure (suction) in unsaturated soil slope is the main reason for slope slide. Even under relatively dry conditions, 60%-77% shear strength of unsaturated soil slopes is provided by negative pore water pressure (suction) (Wang et al. (2021)). Sabrina et al. (2020) and Alfrendo et al. (2021, 2022) et al. believe that considering the SWCC characteristics of unsaturated soil, the slope stability analysis is more consistent with the actual slope environment, and the result is more accurate.

In addition to rainfall, the stability of railway slope is also affected by locomotive vibration (Xu et al. 2017 and Xu et al. 2018), but the harm caused by locomotive vibration does not seem to attract enough attention. According to the investigation of David et al. (2016), Among 1604 railway tracks in 9 countries and regions around the world, 44% of locomotive-induced ground vibration exceeds the threshold requirements of relevant countries. However, the vibration generated by locomotive is different from the pulse vibration caused by explosions and the limited, irregular and random vibration caused by earthquakes. It is a repetitive vibration with "long duration, small amplitude and high frequency". This kind of long-term

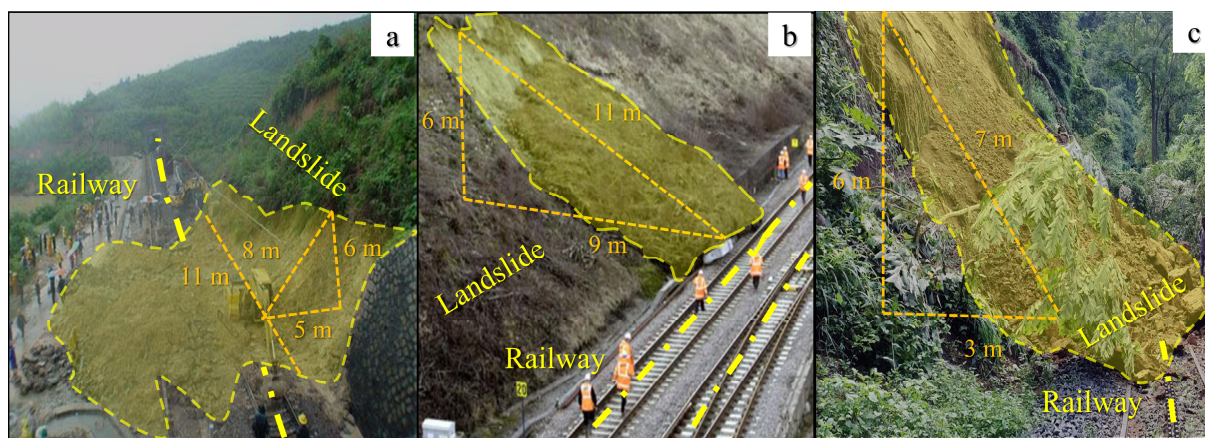


Fig. 1 Landslide caused by rainfall-vibration joint action. (a) Fujian Landslide located in Zhanghuban-Shuangkeng section in Fujian Province, China; (b) Chipping Sodbury Landslide located in Chipping Sodbury, South Gloucestershire, UK; (c) Nilgiri Mountain Landslide located in Kallar-Hillgrove section, India.

cumulative damage is not conducive to the stability of railway slope. Therefore, it is very important to clarify the action characteristics of locomotive vibration on railway slope and understand the failure evolution process of slope to determine the stable stage of railway slope. Yan et al. (2019) took the loess terrace in Qin'an City, Gansu Province in China as the monitoring point to determine the propagation and attenuation characteristics of locomotive acceleration on the loess terrace slope. Georges et al. (2016) and Xie et al. (2021) also determined the variation characteristics of the locomotive acceleration with different slope types as the research objects.

However, the joint effect of multiple factors is not the superposition of the single effect. For example, Ma et al. (2021) found that blasting vibration and rainfall infiltration can both reduce the strength of rock and sand, but the joint effect of water-vibration is more significant than that of a single factor. Besides, Wang (2021) took the railway slope under the joint action of water and vibration as the research object and put forward five effects which are acceleration of cracking, infiltration, disintegration, sliding, and subsidence (referred to as "Five Vibration-induced Effects" for short). The long-duration vibration of the locomotion will accelerate crack expansion and extension (crack-promoting effect). At the same time, the liquid phase inside the slope will accelerate infiltration. Therefore, the gaseous phase will accelerate escape (infiltration-promoting effect), which will lead to the rapid disintegration of the slope surface (disintegration-promoting effect). Therefore, the stability of the slope decreases sharply and it causes the slope to slide rapidly (sliding-promoting effect). In the vertical direction, vibration subsidence and collapsibility will be coupled with each other, resulting in a more obvious settlement (subsidence-promoting effect). The proposal of "Five Vibration-induced Effects" indicates that human beings have formed a comprehensive cognition of the geological disasters caused by the joint action of water and vibration. It also means that it is urgent to explore the internal mechanism of such geological disasters. In the past five years, a series of researches on the crack-promoting, disintegration-promoting and subsidence-promoting effects under the joint action of water and vibration have been completed (Wang 2019a, 2019b, 2019c) and Zhang (2020a, 2020b). However, only by clarifying the unstable process and characteristics of slope under the joint action condition, and clarifying the effect of

rainfall and vibration on slope stability (sliding-promoting effect), can prevent the and control the railway slope slide effectively. But so far, there are very few studies on this part.

In this paper, the special vibration form of "long holding time, small amplitude and high frequency" is taken as the vibration source (the vibration mentioned below is the special vibration of "long holding time, small amplitude and high frequency"). The variations in water content and soil pressure of sandy soil slope under these three conditions are compared and analyzed. Combined with the surface failure phenomenon, the main control factors affecting the stability of slope structure under the joint action are defined. And the causes of slope instability induced by each control factors are clarified. The unstable evolution process of the unsaturated soil slope under the joint action of rainfall-vibration is determined. The research results obtained in this paper reveal the unstable evolution of joint action of rainfall-vibration and lay a solid theoretical foundation for the early warning and prevention technology of such geological disasters.

2 Materials and Methods

2.1 Soil sample

To simplify the analysis of the unstable evolution process, a soil sample with minimal cohesion is chosen. According to Zhang et al. (2011), the variation coefficient of soil shear strength may reach 20% to 30%. The selected soil sample (Fig. 2a), matches the model test requirements, with a low variation coefficient of average shear strength (11.0%) and suitable gradation (Table 1). Classified as sandy soil according to Atterberg's standard, its maximum particle size is less than 1.3mm, with a non-uniformity coefficient (C_u) of 1.63 and curvature coefficient (C_c) of 1.00. To assess slope stability under different conditions, the (dynamic) permeability coefficient and soil water characteristic curve (SWCC) are determined through permeability experiments and sensor data. See Table 2 for specific parameters.

2.2 Instruments

This paper investigates the unstable evolution resulting from the joint action of rainfall and vibration on railway slopes through model tests. The model test

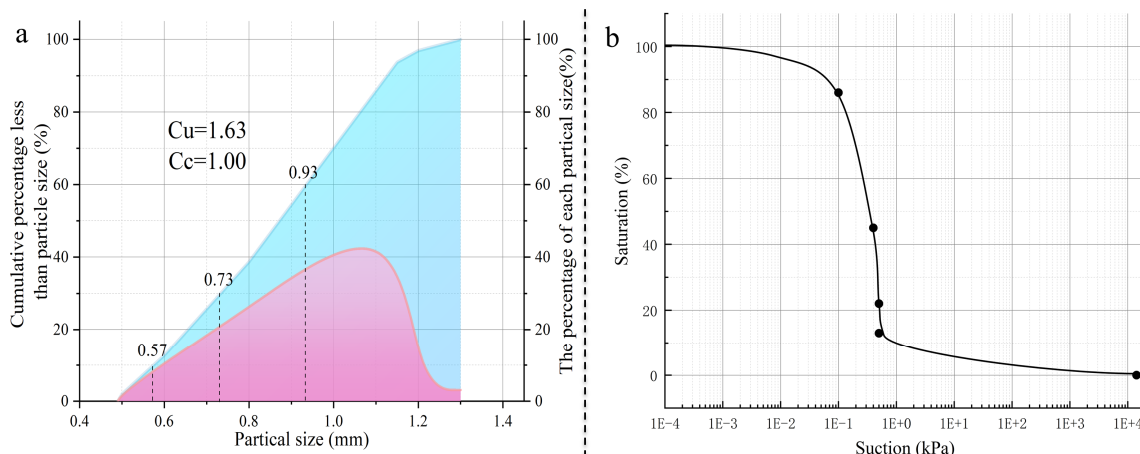


Fig. 2 Related parameters of the soil sample. (a) Gradation curve of soil sample; (b) SWCC of soil sample; (c) Physical property parameters of soil sample.

can be divided into full-scale model test (Pesci et al. 2022; Luisa et al. 2023), n-g centrifuge test (Xu et al. 2022; Yang et al. 2023) and 1-g scale model test (Ha et al. 2023). However, due to resource constraints, the 1-g scale model is chosen as the primary testing method.

Table 1 Comparison of shear strength parameters between model test and prototype slope.

Parameters	Prototype slope	Model test	CV	
Density (g/cm ³)	1.87	1.82		
Cohesion (kPa)	21.9	2.2		
Internal friction angle (°)	29.0	37.5		
Shear stress (kPa/m ²)	at 3m	53.0	44.1	16.8%
	at 6m	84.1	86.0	2.3%
	at 9m	115.1	127.9	11.1%
	at 12m	146.2	169.8	16.1%
	at 15m	177.3	211.7	19.4%
Mean shear stress (kPa/m ²)	115.1	127.9	11.1%	

Note: CV, Coefficient of variation

Table 2 Physical property parameters of soil sample.

Physical property parameters	Data
Dry density, ρ_d (g/cm ³)	1.65
Natural density, ρ (g/cm ³)	1.82
Water content, ω (%)	10
Void ratio, e	0.6
Relative density, G_s	2.65
Permeability coefficient, k (cm/s)	1.26E-4
Dynamic permeability coefficient, k_d (cm/s)	3.26E-2

The model consists of a cuboid acrylic box (102 cm×102 cm×61 cm) to replicate the slope’s geometry, a vibration exciter designed for “long duration, low amplitude, and high frequency” vibrations, atomizer devices for rainfall simulation, and data acquisition tools for monitoring soil pressure and water content. To prevent particle and water leakage and maintain

box rigidity, a 1mm rubber film is wrapped around the outside of the model box. The specific model test device is shown in Fig. 3.

In the aspect of boundary conditions, the model test learns the methods used by Fan (2016), Yang (2020) and Xue (2020) for reference. 15 mm foam plastic and rubber plates are laid on the back and the bottom of both sides of the acrylic plate respectively, which are used as damping materials together to reduce the influence of boundary reflection waves on the slope. The vibration waveform simulated by the exciter is shown in Fig. 3d. The simulated waveform is completely consistent with the basic requirement, as reported by Wang et al. The FCV (flow control valve) included in the atomizer can adjust the rainfall intensity and ensure the stability of rainfall intensity. While the atomizing nozzle can reduce the surface runoff and ensure that the failure of slope is mainly caused by infiltration of rainwater.

Due to the limited size of the scaled model, it's impractical to embed a large number of sensors, especially for monitoring pore water pressure directly. Therefore, it is necessary to reflect the change trend of pore water pressure indirectly through limited sensors. Studies by Sun (2019), Wu (2020), and Tran (2021) indicated that increased water content leads to higher pore water pressure, reducing the slope's effective stress and inducing landslides. Therefore, in the 1-g scale model tests, we analyze pore water pressure trends indirectly through water content variations to assess slope stability. All sensor parameters are listed in Table 3, and calibration is performed before testing. Water content sensors are calibrated using known soil samples, and deviations are corrected. Soil pressure sensors measure total pressure and are calibrated to

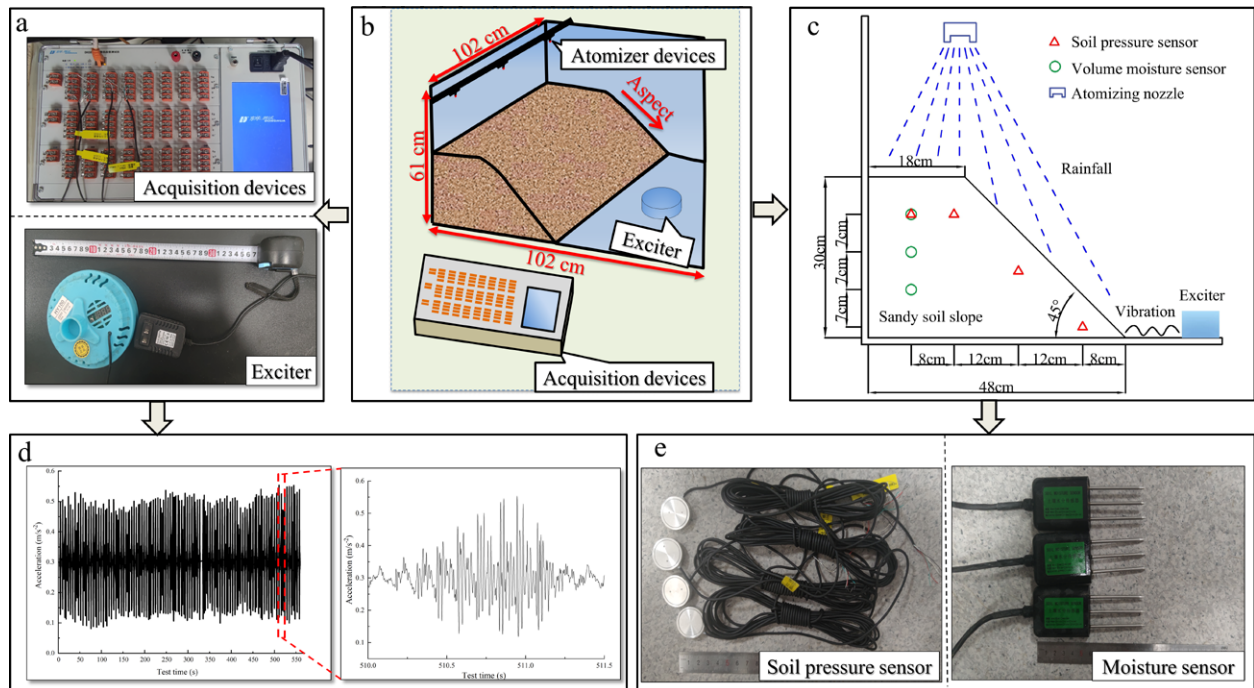


Fig. 3 Test design diagram. (a) Test equipment; (b) Diagram of the model test; (c) Section diagram of the model test; (d) Vibrational waveform of exciter; (e) Test sensors.

Table 3 Main parameters of the sensors used in the experiment.

Information	Moisture sensor	Soil pressure sensor
Product model	RS-SD-No1	BW-28
Measuring range	0%-100%	0-30 KPa
Accuracy	2.0% FS	0.5% FS
Resolution	0.1%	0.2% FS
Manufacturer	Zhiyuan/China	Jincheng/China

ensure accuracy. Pre-tests are conducted to verify sensor range and precision, ensuring repeatable test results.

2.3 Scheme of test

Following the findings by Zhan et al. (2020), the test is based on a railway landslide located in Fugu County, Yulin City, Shaanxi Province. The railway cutting at this site has a height ranging from 6 to 18 meters with an approximate slope of 45°, lacking protective measures. Following the emergence of numerous tension cracks, different degrees of slope movement are observed, eventually resulting in a landslide. To simulate this case, a 1-g scale model test is conducted based on similarity principles, reducing or enlarging factors in proportion according to three similarity criteria. 1-g scale model test is based on the

similarity principle. Xue et al. (2020) clarified the failure mechanism of underground loess caverns through 1:5 scale model test, while Chen et al. (2020) explored the effects of rainfall duration before earthquakes on low-angle loess slopes through a 1:10 scale model test. Feng et al. (2018) studied anti-dip rock slope dynamic responses via a 1:100 scale model test. For this test, a 1-g scale model with a 1:50 scale coefficient is designed, aligning with the landslide scaling coefficient (1:50) proposed by Wang et al. (2021). The slope angle is set at 45° under various simulation conditions. The model comprises a single-step scale model with dimensions of 100 cm in length, 30 cm in height, 18 cm in top width, and 48 cm in bottom width. The proportional coefficients of other parameters are detailed in Table 4, while specific parameters are illustrated in Fig. 3.

To ensure comprehensive rainfall coverage, the atomizing nozzle is positioned approximately 24 cm from the slope’s top. Heavy rain simulation is employed with an average rainfall of 0.16 mm/min, falling within the range of 100 mm to 249.9 mm in 24 hours, classified as heavy rain by the National Meteorological Administration of China. Soil pressure and volume moisture sensors are strategically placed throughout the slope model under three conditions: vibration, rainfall, and their joint action. Soil pressure

Table 4 The scale factor of model tests

Variable	Para.	Similarity	Scale factor
Length	L	C_L	0.02
Displacement	X	$C_L=C_X$	0.02
Elastic modulus	E	C_E	2
Poisson ratio	μ	C_μ	1
Strain	ε	$C_\varepsilon=\Delta C_X/C_X$	1
Stress	σ	$C_\sigma=C_E C_\varepsilon$	2
Acceleration	a	C_a	100
Mass	M	$C_M=C_L C_a^2/C_a$	0.000008
Equivalent density	ρ	$C_\rho=C_M/C_L^3$	1
Gravity acceleration	g	C_g	1
Gravity	G	$C_G=C_M C_g$	0.000008
Cohesion	c	C_c	0.05
Internal friction angle	φ	C_φ	1.29

Note: Para., Parameter.

sensors are positioned at the slope’s top, shoulder, waist, and toe, while volume moisture sensors are distributed at the slope’s upper, middle, and lower sections. The specific distribution scheme is shown in Fig. 3c.

Monitoring commences after slope accumulation and continues for about two weeks until data from all sensors stabilize. Following stabilization, formal testing begins. Data on soil pressure and water content are collected under vibration, rainfall, and joint conditions. The slope angle and compactness are based on actual loess cutting slope parameters. Slope mass is determined by test-designed density and volume, with soil compaction performed until reaching a 5 cm height. Testing proceeds under each condition until slope damage occurs or local soil pressure data stabilize for over 10 minutes. Observations of slope failure under the three conditions are recorded using a Canon EOS 5D Mark IV camera at different stages.

3 Testing Results

3.1 Failure phenomena of sandy soil slope

Fig. 4 illustrates the failure phenomena of sandy soil slopes under different conditions. The slope failure phenomena caused by vibration, rainfall, and rainfall-vibration joint action are not completely the same. Vibration induces surface particle sliding and accumulation at the slope’s toe (Fig. 4a), primarily occurring at the start of vibration. Rainfall generates micro-cracks less than 1mm wide on the slope surface, accompanied by turbid water seepage (Fig. 4b). Additionally, after collecting the exudation and sitting aside for a period, micro-particle deposition at the beaker bottom becomes visible.

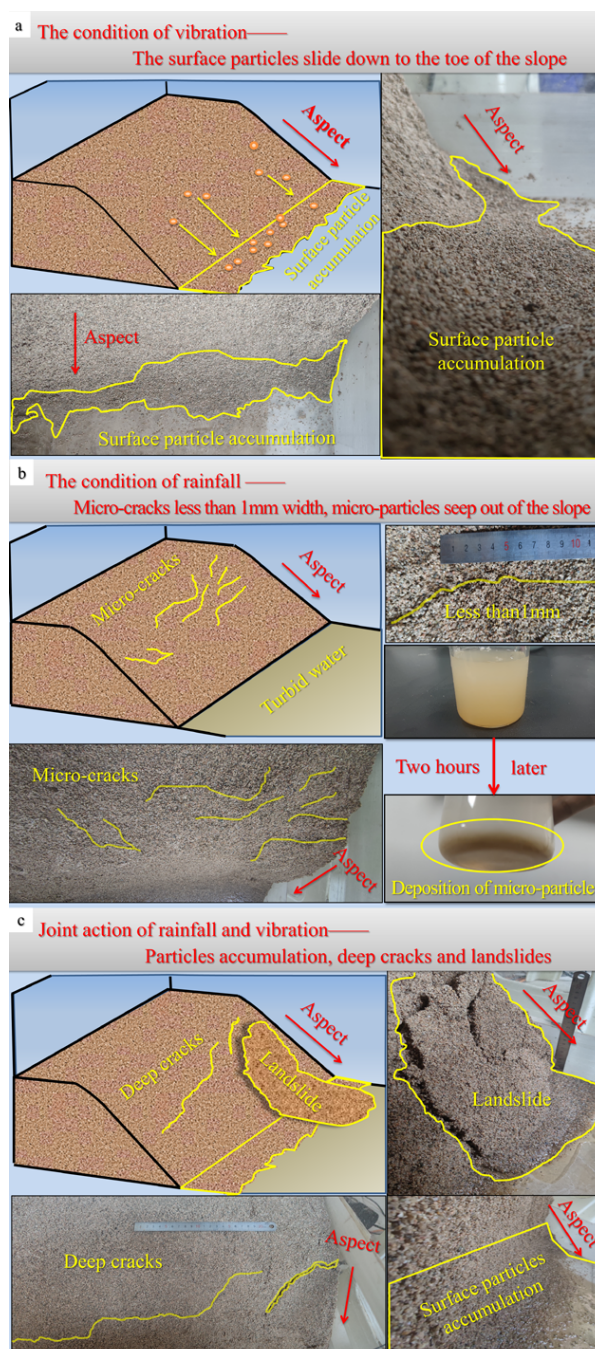


Fig. 4 Failure phenomenon of the slope caused by (a) Vibration; (b) Rainfall; (c) Joint action of rainfall-vibration.

Comparing failure phenomena under the three conditions reveals similarities and differences. Initially, joint action mimics single-factor actions, with surface particles sliding to the slope's toe, akin to the vibration condition. Subsequently, micro-cracks gradually develop on the slope surface, consistent with rainfall-induced failures. Under joint action, early-stage micro-cracks continue expanding, forming deep cracks.

Continuous joint action prompts temporary local slope sliding, leading to landslide formation. The sliding surface spans from the shoulder to the toe of the slope, transitioning from a near 90° angle at the shoulder to 45° at the waist (Fig. 4c).

During the model test, soil pressure curves exhibit sudden violent fluctuations. To investigate, the slope's lateral side is cut before failure. Inspection reveals penetrated internal cracks and formed failure parts, evident in Fig. 5.

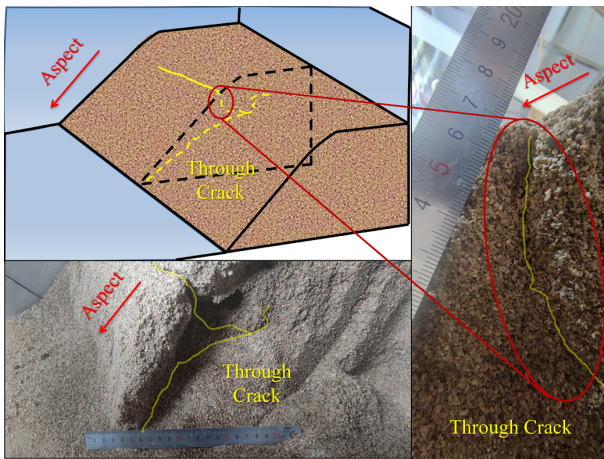


Fig. 5 Penetrated internal cracks in the non-sliding body.

3.2 Response law of internal parameters

In the model test, the soil pressure sensor monitors changes in the total stress of the overlying soil, encompassing increments in self-weight stress during soil humidification, as well as increases in pore pressure due to vibration, rainfall, and vibration force. The increment of self-weight pressure during soil humidification can be calculated using Eq. (1). For instance, at the slope shoulder, increases of 0, 0.12 kPa, and 0.09 kPa are observed under vibration, rainfall, and joint action conditions, respectively.

$$\Delta\sigma_1 = \frac{\omega_3 - \omega_2}{1 + \omega_1} * \rho gh \quad (1)$$

where $\Delta\sigma_1$ is the increment of self-weight stress in the process of soil humidification; ω_1 , ω_2 and ω_3 are the test design water content (10% is taken), the initial water content of the slope measured before the rainfall and the final water content of the slope after rainfall respectively; ρ is the test design density and 1.82 g/cm is taken in the test; g is the acceleration of gravity, taken as 10 N/kg; h is the depth of the calculated point

The infiltration force of the rainwater can be computed according to Eq. (2). For instance, at the

shoulder stress point, the infiltration force is 0, 0.65kPa and 0.01kPa respectively.

$$\Delta\sigma_2 = \frac{\gamma_w hv}{k} \quad (2)$$

$\Delta\sigma_2$ is the increment of soil stress caused by infiltration force; γ_w is bulk density and 10 kPa is taken in the test; v is infiltration velocity of rainwater; k is the permeability coefficient, which is 1.26E-4 cm/s under static condition and 3.26E-2 cm/s under vibration condition.

According to the above formulas and the characteristics of soil pressure curves under different conditions, the variation of pore pressures caused by vibration and rainfall can be determined more accurately.

The monitoring results reveal the following observations:

Under vibration conditions, the water content of the slope remains relatively stable (Fig. 6). However, the variation trend of soil pressure across different

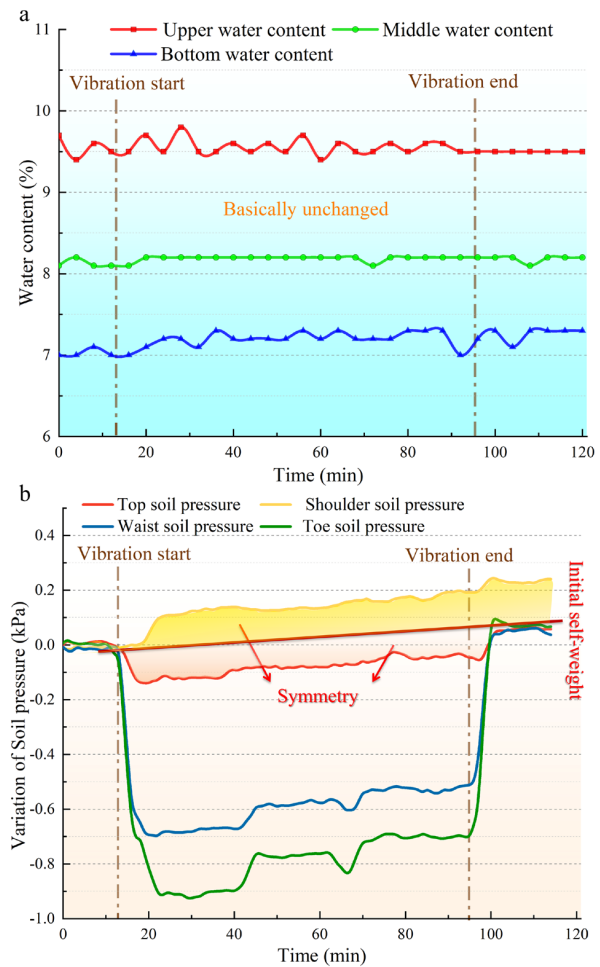


Fig. 6 Response law of internal parameters under the influence of vibration. Variation curve of (a) water content and (b) soil pressure.

parts of the slope exhibits notable disparities. Taking the stress at the slope shoulder as an example, the dynamic pore pressure from the top of the slope to the toe of the slope are 0.1kPa, 0.1kPa, 0.9kPa and 0.7kPa respectively. With the beginning of vibration, soil pressure undergoes rapid changes across all slope sections simultaneously. Overall, the soil pressure curves at adjacent positions, such as the top and shoulder parts, exhibit symmetrical patterns. Symmetry is determined using the line close to the initial self-weight pressure (the X-axis) as the symmetry line. Notably, the variation trends of soil pressure at the top and shoulder parts appear symmetrical (as depicted by the orange and red parts in Fig. 6b). As shown in Eq. (3),

$$\Delta Pt = mv_1 - mv_0 \quad (3)$$

where ΔP is the change of soil pressure caused by vibration; t is time; m is the local quality of the slope; v_0 and v_1 are the initial velocity of local particles on the slope and the velocity caused by vibration, respectively.

When vibration occurs, particles at the slope's top and shoulder experience an impulse of equal magnitude but opposite direction. This results in the movement of particles away from the top and toward the shoulder. Consequently, vibration induces two distinct effects on the slope: a densification effect and a loosening effect. These effects are explained by the particle contact structure proposed by Dong et al. (2022). With the stop of vibration, the effect disappears, the vibration loosening area gradually recovers, but the vibration densification area doesn't change. the loosening effect gradually recovers, while the densification effect remains unchanged. Since there are no violent fluctuations during vibration, it can be inferred that the dynamic pore pressure generated by the vibration, rather than the vibration force itself, is responsible for this phenomenon.

As depicted in Fig. 7, under rainfall conditions, the water content across different parts of the slope exhibits a similar trend, albeit with varying start times. Initially, the water content at the top of the slope increases sharply and reaches its peak rapidly. Subsequently, the middle and bottom sections of the slope experience delayed increases, occurring 5 and 20 minutes later, respectively.

Concurrently, soil pressure across the slope gradually increases, starting from the onset of rainfall. This rise in soil pressure is consistent with the water content changes. Successively, soil pressure increases at the top, shoulder, waist, and toe of the slope.

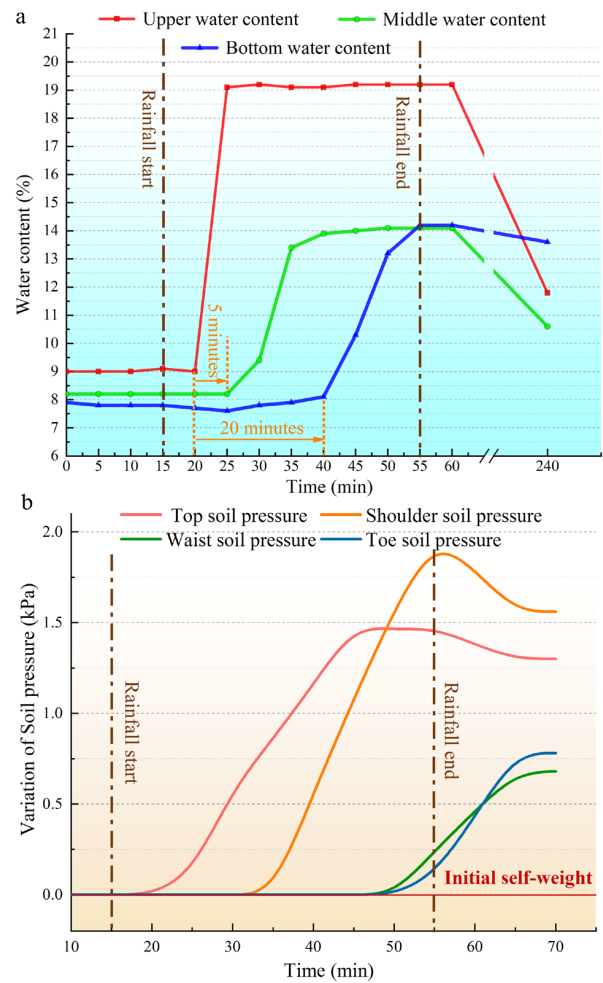


Fig. 7 Response law of internal parameters under the influence of rainfall. Variation curve of (a) water content and (b) soil pressure.

Comparatively, the time frame for soil pressure changes during rainfall is longer, typically lasting several hours, with a larger magnitude of up to 2 kPa. Additionally, the excess pore water pressure induced by rainfall diminishes as infiltration depth increases. For instance, at the slope shoulder, the excess pore water pressure reaches approximately 1.1 kPa. While excess pore water pressure can also arise under vibration conditions, its magnitude is comparatively minor. For instance, at the slope shoulder, the excess pore water pressure induced by vibration is approximately 0.1 kPa, as observed in Fig. 6.

Under joint action, the water content variation in the slope mirrors that observed during rainfall. As depicted in Fig. 8a, there is a rapid increase in water content at the slope's top at the onset of rainfall, followed by delayed increases at the middle and bottom sections, occurring 5 minutes later. Notably, the infiltration rate under joint action is four times

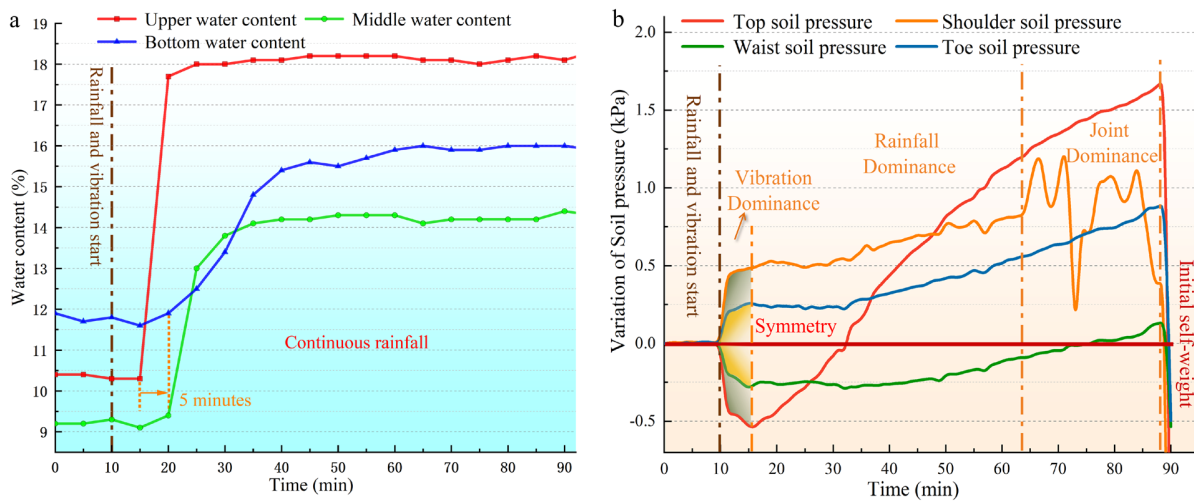


Fig. 8 Response law of internal parameters under the influence of rainfall-vibration joint action. Variation curve of (a) water content and (b) soil pressure.

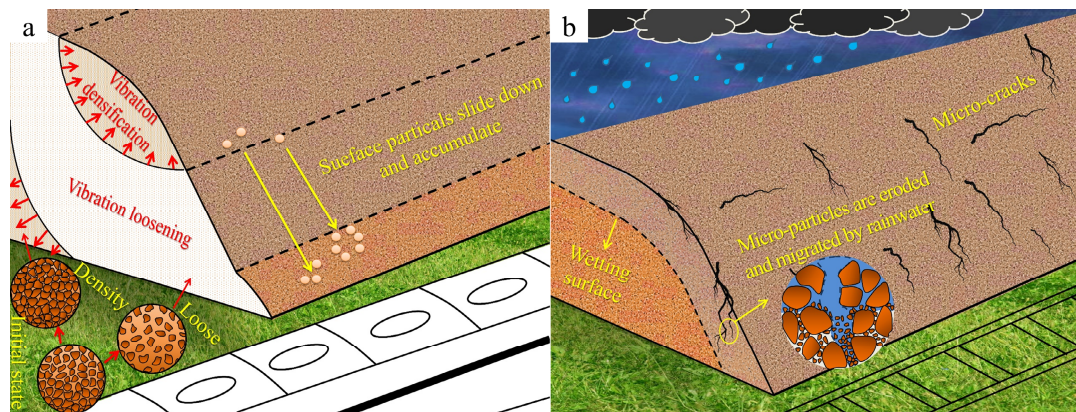


Fig. 9 Failure mode of slope under vibration condition (a) and rainfall condition (b).

faster than that under rainfall conditions.

Regarding soil pressure dynamics, the variation range does not exceed 0.5 kPa, and changes occur within one minute. At the initiation of joint action, with the initial self-weight pressure as the axis of symmetry, soil pressures at corresponding locations (top and shoulder, waist and toe) exhibit symmetrical patterns, as illustrated in the green and orange projections in Fig. 8b. This phenomenon resembles the variation in soil pressure induced by vibration alone, indicating that dynamic pore pressure generated by vibration contributes to both densification and loosening areas of the slope under joint action.

Subsequently, soil pressure trends align closely with those observed during rainfall conditions. However, a notable difference emerges: as soil pressure continues to rise, the shoulder soil pressure experiences abrupt fluctuations akin to a cliff before each pressure decrease.

4 Discussion

4.1 Failure characteristics of sandy slope under vibration

From what has been discussed above, the dynamic pore pressure induced by vibration triggers both loosening and densification effects in the slope, working in tandem. As shown in Fig. 9a. This simultaneous effect of vibration loosening and vibration densification is the failure characteristic of sandy soil slope caused by vibration. The corresponding internal response law of slope is the symmetrical variation phenomenon of soil pressure. The corresponding failure phenomenon is the slope particles slide down and accumulate under the toe of slope.

Analysis of the whole trend of soil pressure, it can be known that the dynamic pore pressure caused by vibration is instantaneous when the vibration starts

and ends, and does not change during the period. Compared with rainfall, the dynamic pore pressure is smaller which does not exceed 1 kPa. And the time of such change is only within one minute. This is the variation characteristic of dynamic pore pressure caused by vibration.

4.2 Failure characteristics of sandy slope under rainfall

Due to the infiltration force in the rainfall condition is much greater than the other conditions, the micro-particles deposited in the beaker. Because of this reason, several micro-cracks less than 1mm in width generate on the slope surface which is totally different from deep cracks under joint action. Such micro-cracks with a width less than 1mm are one of the failure characteristics of sandy soil slopes under the condition of rainfall in this model test. Its failure mode is shown in Fig. 9b.

Compared with the instantaneous dynamic pore pressure caused by vibration, the excess pore water pressure caused by rainfall on the soil pressure usually takes several hours. In this model test, the effect of rainfall on the slope is also about one hour. And compared with the dynamic pore pressure, the excess pore water pressure is more significant. In this model test, the variation range of excess pore water pressure can be up to 2 kPa. The large and long time pore pressure change is the variation characteristics of excess pore water pressure.

4.3 Unsaturated soil slope stability formula considering the influence of rainfall and vibration

According to the stability formula of unsaturated soil slope proposed by Vanapalli and the soil pressure data under the joint condition, the stability coefficient of slope is only 1.2. It is not consistent with the actual failure phenomenon of slope. The reason is that it is not considered the dynamic pore pressure u_d generated by vibration and the excess pore water pressure u_w generated by heavy rainfall. In order to consider the impact of vibration and rainfall on the stability of the slope, the stability formula is improved. The model test is checked by the improved stability formulas. The improved formulas are shown in Eqs. (4)-(6).

The shear strength of unsaturated soil slope is mainly composed of effective cohesion c' , internal

friction force and shear strength c_s caused by negative pore water pressure (suction) ψ .

$$\tau_f = c' + (\sigma \cos \alpha - u_a - u_d - u_w) \tan \varphi' + c_s \quad (4)$$

where c' and φ' are the effective cohesion and internal friction angle of saturated soil respectively, 2.2 kPa and 37.5° are taken in the test respectively); $(\sigma - u_a - u_d - u_w)$ is the normal stress, where σ is the slope self-weight stress, u_a is the pore gas pressure (Since the test material is sandy soil, its pores can be considered to be connected with the atmosphere, so the pore gas pressure is taken as 0), α is the sliding angle of the sliding surface.

The shear strength c_s induced by negative pore water pressure (suction) is related to the saturation S of the monitoring point

$$c_s = \psi S \tan \varphi' \quad (5)$$

$$S = \frac{wG_s}{e} \quad (6)$$

here w is the water content, G_s is the relative density (2.65g /cm is taken in this test), e is the porosity ratio (0.6 is taken in this test)

The shear force of the unsaturated soil slope can be roughly divided into two parts: the shear force generated by the slope's self-weight σ and the shear stress generated by the vibration force τ_d . The stability formula of the sandy soil slope under the condition of locomotive vibration can be calculated by obtaining the slope stability coefficient FOS according to the ratio of shear strength to shear stress, as shown in Eq. (7)

$$FOS = \frac{\sum_i [(\tau_f + \sigma_d \cos \alpha \tan \varphi) L]_i}{\sum_i [(\sigma + \sigma_d) \sin \alpha L]_i} \quad (7)$$

In Eq. (7), τ_f , σ_d , σ , φ , L and α refer to the shear strength, vibration shear stress, self-weight shear stress, internal friction angle, length of sliding surface and sliding angle of the unsaturated soil slope corresponding to the i block respectively.

Taking the sliding surface at the slope shoulder under the joint action condition as an example, the stability coefficients of unsaturated soil slope under the initial condition, vibration condition, rainfall condition and joint action are 1.86, 1.75, 1.06 and 0.99 respectively. It can be seen that both vibration and rainfall will reduce the stability of the slope. However, the dynamic pore pressure generated by vibration is small and has little influence on the stability of the slope. The excess pore water pressure generated by rainfall is a long-term cumulative force, and the shear strength of the slope is significantly reduced under the influence of heavy rainfall. Considering the erosion and migration of

rainwater, it can be seen that as long as the time is long enough, the slope will eventually slide.

4.4 Unstable evolution of sandy slope under joint action

The joint effect of vibration and rainfall on slope stability reveals critical factors. Initially, soil pressure variations at different parts of the slope are symmetrical (as shown in the green projection and the orange projection in Fig. 8b). In addition, the variation range of soil pressure is only 0.4 kPa and the change time is only within one minute. This kind of small amplitude and instantaneous symmetry phenomenon proves that the increasing soil pressure is mainly caused by the vibration dynamic pore pressure. At the same time, the sliding particles on the slope is also like the phenomenon under vibration condition. This suggests that vibration plays a greater role than rainfall in increasing soil pressure, impacting slope stability. However, as rainfall persists, symmetrical soil pressure variations disappear, and pressures on the slope increase sequentially. Particularly, soil pressure at the top continues to rise significantly over time, exceeding 2 kPa within an hour. This, coupled with observed micro-cracks, indicates that rainfall has become the primary destabilizing factor for sandy soil slopes, replacing the influence of vibration.

Since the micro-cracks generated, a portion of the energy generated by vibration has an effect on the crack surface (Hu et al. 2018; Davies et al. 2019; Lin et al. 2020; Li et al. 2019), the soil pressure of this part is more sensitive to the impact of vibration. The micro-cracks continue to expand and form deep cracks. As these micro-cracks expand into deep cracks, the soil pressure on the slope shoulder experiences sudden and violent fluctuations, indicating a vibration force of approximately 0.4 kPa. Despite the joint action resulting in a lower pore pressure increment compared to rainfall alone, the slope stability coefficient drops to 0.99, indicating slope damage and accelerated sliding. This is evidenced by almost

complete crack penetration and slope sliding within 20 minutes, mirroring prototype behavior. Thus, under rainfall-vibration joint action, the appearance of deep cracks and significant soil pressure fluctuations signify crack penetration and slope instability (Fig. 10).

In summary, under rainfall-vibration joint action, the slope undergoes three unstable stages: rainfall erosion cracking, vibration-induced penetration, and slope instability sliding. Throughout this process, dynamic pore pressure from vibration amplifies excess pore water pressure from heavy rainfall, exacerbating slope instability. Prolonged heavy rainfall, coupled with erosion and water migration, leads to slope

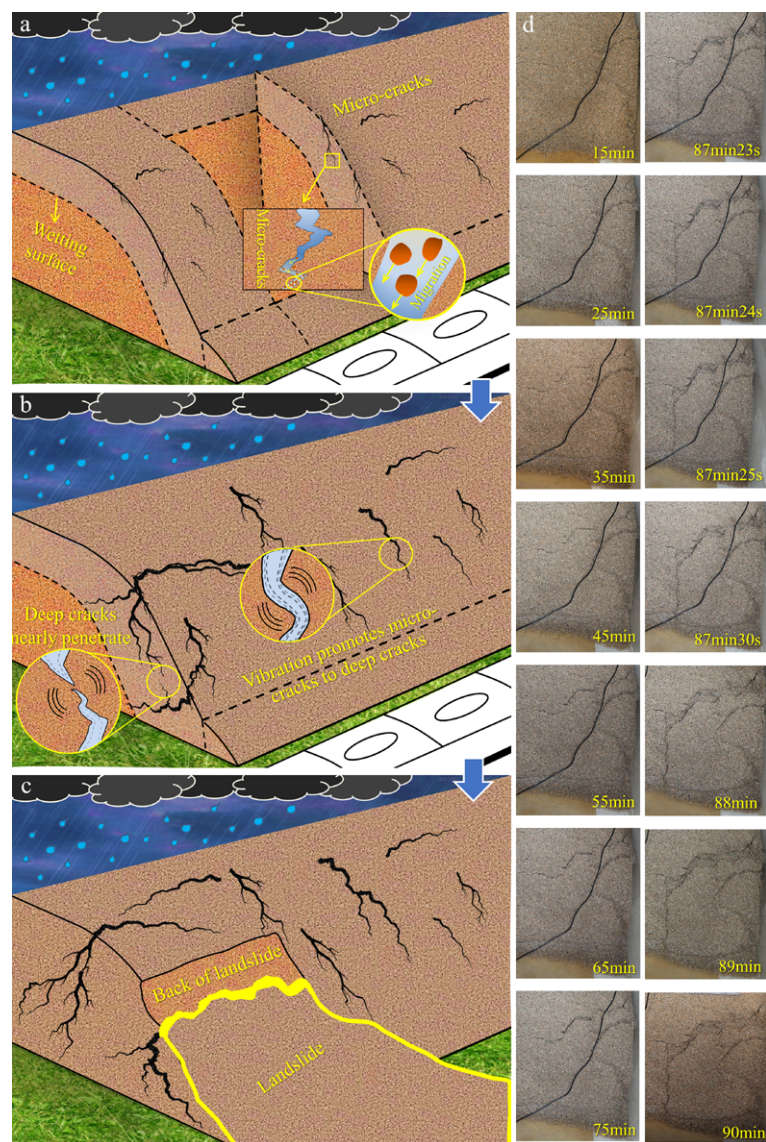


Fig. 10 Failure mode of slope under rainfall-vibration joint action: (a) Rainfall erosion cracking stage; (b) Vibration promotion penetrating stage; (c) Slope instability sliding stage; (d) Unstable evolution under rainfall-vibration joint action.

cracking, resulting in inevitable instability and sliding. Additionally, as cracks form, vibration force significantly increases, accelerating slope sliding. In essence, vibration promotes sliding while rainfall induces it.

However, the model test simplifies conditions by using sandy soil with minimal cohesion, which may not fully represent actual railway slopes. The improved stability formula for unsaturated soil slopes is theoretical and is only applied here for verification. Future studies aim to enhance understanding by monitoring parameters such as strain, stress, and pore pressure on real railway slopes under vibration-rainfall conditions. This will help validate the improved stability formula and guide further research efforts.

5 Conclusion

In this paper, by simulating the special vibration form of the locomotive with "long duration, small amplitude, and high frequency", the model test of sandy soil slope under three conditions of rainfall, vibration, and rainfall-vibration joint action is carried out. The following conclusions are drawn from the test:

1. The unstable evolution process of sandy soil slope, under the rainfall-vibration joint action, can be divided into rainfall erosion cracking, vibration promotion penetrating, and slope instability sliding three stages. Rainfall induces micro-cracks, which continue to expand under vibration until deep cracks are formed, leading to instantaneous slope instability.
2. The generation of deep cracks and the violent fluctuation of soil pressure constitute the unstable characteristics of sandy soil slopes. Under the influence of vibration, micro-cracks continue to expand, forming deep cracks. The effect of vibration force on slope will increase significantly at this time. The corresponding variation characteristic of soil pressure is such violent fluctuation. And the corresponding failure phenomenon is deep cracks.
3. Vibration promotes sliding, while rainfall induces sliding by generating excess pore water pressure. Dynamic pore pressure reduces the shear strength of the slope, while excess pore water pressure

References

- Alfredo S, Martin W, Qian Z, et al. (2021) Stability and consolidation of sediment tailings incorporating unsaturated soil mechanics. *Fluids* 6:423-439.
<https://doi.org/10.3390/fluids6120423>
- Alfredo S, and Harianto R (2022) Role of unsaturated soil properties in the development of slope susceptibility map. *PI Civil*

from rainfall further reduces the safety factor of the slope. Rainwater erosion leads to cracking, providing the basis for sliding surfaces, while continuous vibration accelerates the formation of weak surfaces and accelerates slope sliding.

These research conclusions reveal the unstable evolution of sandy soil slopes under rainfall-vibration joint action, aiming to provide a theoretical basis for early warning and prevention technology of railway slopes. However, it is noted that this study is limited to sandy soil slopes without cohesion and is based on model tests, which may not completely replicate real failure processes of railway slopes. Future research will aim to address these limitations.

Acknowledgments

The work in this study was supported by the Major Research Plan of the National Natural Science Foundation of China (Grant No. 42027806), the Key Programme of the Natural Science Foundation of China (Grant No. 41630639) and National Natural Science Foundation of China General Program (Grant No. 42372324).

Author Contribution

DONG Haoyu: Investigation, Data curation, Conceptualization, Formal analysis, Writing-original draft, Writing-review & editing. WANG Jiading: Funding, Writing-review & editing, Conceptualization, Supervision. ZHANG Dengfei: Funding, Conceptualization, Writing-review & editing, Supervision. LI Lin: Visualization, Formal analysis. XU Yuanjun: Investigation, Visualization, Methodology.

Ethics Declaration

Availability of Data/Materials: The datasets generated during this study are available from the corresponding author upon reasonable request and within the framework of cooperation agreements and scientific research projects.

Conflict of Interest: The authors declare no conflict of interest.

- Eng-Geotec 175: 276-288.
<https://doi.org/10.3390/fluids6120423>
- Chen JC, Wang LM, Pu XW, et al. (2020) Experimental study on the dynamic characteristics of low-angle loess slope under the influence of long- and short-term effects of rainfall before earthquake. *Eng Geol* 273:105684.

- <https://doi.org/10.1016/j.enggeo.2020.105684>
- David PC, Grzegorz PM, Georges K, et al. (2016) The growth of railway ground vibration problems - a review. *Sci Total Environ* 15:1276-1282. <https://doi.org/10.1016/j.scitotenv.2015.09.101>
- Dong HY, Wang JD, Zhang DF, et al. (2022) Microscopic mechanism angle of repose in friable loess and its relationship with slope angle. *Front Earth Sci* 9:128-139. <https://doi.org/10.3389/feart.2021.777467>
- Fan G, Zhang JJ, Wu JB, et al. (2016) Dynamic response and dynamic failure mode of a weak intercalated rock slope using a shaking table. *Rock Mech Rock Eng* 49:3243-3256. <https://doi.org/10.1007/s00603-016-0971-7>
- Feng XX, Jiang QH, Zhang XB, et al. (2018) Shaking table model test on the dynamic response of anti-dip rock slope. *Geotech Geol Eng* 37:1211-1221. <https://doi.org/10.1007/s10706-018-0679-4>
- Georges K, David PC, Bryan O, et al. (2016) Railway cuttings and embankments: experimental and numerical studies of ground vibration. *Sci Total Environ* 557-558:110-122. <https://doi.org/10.1016/j.scitotenv.2016.03.016>
- Ha L, Oh I, Yoo M (2023) Analysis of factors affecting railway settlement of embankment section due to liquefaction using 1-g shaking table model tests. *Geotech Eng* 27(7):2822-2833. <https://doi.org/10.1007/s12205-023-2133-2>
- He K, Ma GT, Hu XW, et al. (2019) Characteristics and mechanisms of coupled road and rainfall-induced landslide in Sichuan China. *Geomat Nat Haz Risk* 10:2313-2329. <https://doi.org/10.1080/19475705.2019.1694230>
- Hou TS, Duan X, Liu HY (2021) Study on stability of exit slope of chenjiapo tunnel under condition of long-term rainfall. *Environ Earth Sci* 80:590-607. <https://doi.org/10.1007/s12665-021-09895-x>
- Hu YG, Liu MS, Wu XX, et al. (2018) Damage-vibration couple control of rock mass blasting for high rock slopes. *Int J Rock Mech Min* 103:137-144. <https://doi.org/10.1016/j.ijrmmms.2018.01.028>
- Kim KS, Jeong SW, Song YS, et al. (2021) Four-year monitoring study of shallow landslide hazards based on hydrological measurements in a weathered granite soil slope in South Korea. *Water* 13:2330-2351. <https://doi.org/10.3390/w13172330>
- Li P, Guo M, Liu SJ, et al. (2019) Dynamic response of loess stepped slopes subjected to vehicle vibration. *J Highw Transp* 13:33-43. <https://doi.org/10.1061/jhtreq.0000689>
- Li Q, Wang YM, Zhang KB, (2022) Failure mechanism of weak rock slopes considering hydrological conditions. *KSCE J Civ Eng* 26:685-702. <https://doi.org/10.1007/s12205-021-1198-z>
- Lin QW, Cheng QG, Li K, et al. (2020) Contributions of rock mass structure to the emplacement of fragmenting rockfalls and rockslides: insights from laboratory experiments. *J Geophys* 125. <https://doi.org/10.1029/2019JB019296>
- Luisa B, Luigi DS, Michalis F, et al. (2023) Seismic assessment of free-standing artifacts: full-scale tests on large shake table. *Earthq Eng Struct D* 52:2708-2730. <https://doi.org/10.1002/eqe.3890>
- Ma CY, Wu L, Sun M, et al. (2021) Failure mechanism and stability analysis of bank slope deformation under the synergistic effect of heavy rainfall and blasting vibration. *Geotech Geol Eng* 39:5811-5824. <https://doi.org/10.1007/s10706-021-01868-y>
- Ma GT, Hu XW, Yin YP, et al. (2018) Failure mechanisms and development of catastrophic rockslides triggered by precipitation and open-pit mining in Emei, Sichuan, China. *Landslides* 15:1401-1414. <https://doi.org/10.1007/s10346-018-0981-5>
- Pesci A, Teza G, Loddio F, et al. (2022) Remote sensing of induced liquefaction: TLS and SFM for a full-scale blast test. *J Surv Eng* 148. [https://doi.org/10.1061/\(asce\)su.1943-5428.0000379](https://doi.org/10.1061/(asce)su.1943-5428.0000379)
- Sabrina CYI, Harianto R, and Alfredo S (2020) Three-dimensional slope stability analysis incorporating unsaturated soil properties in Singapore. *Georisk* 15:202-217. <https://doi.org/10.1080/17499518.2020.1737880>
- Sun P, Wang G, Wu LZ, et al. (2018) Physical model experiments for shallow failure in rainfall-triggered loess slope, Northwest China. *Bull Eng Geol Environ* 78:4363-4382. <https://doi.org/10.1007/s10064-018-1420-5>
- Tran TV, Hung HV, Pham HD, et al. (2021) A non-linear, time-variant approach to simulate the rainfall-induced slope failure of an unsaturated soil slope a case study in Sapa, Vietnam. *J Disaster Res* 16:512-520. <https://doi.org/10.20965/jdr.2021.p0512>
- Wang CT, Wang H, Qin WM, et al. (2021) Experimental and numerical studies on the behavior and retaining mechanism of anchored stabilizing piles in landslides. *Bull Eng Geol Environ* 80:7507-7524. <https://doi.org/10.1007/s10064-021-02391-3>
- Wang HJ, Sun P, Wang G, et al. (2021) Experimental and numerical study of shallow loess slope induced by irrigation. *Catena* 206. <https://doi.org/10.1016/j.catena.2021.105548>
- Wang JD, Gu TF, Zhang MS, et al. (2019a) Experimental study of loess disintegration characteristics. *Earth Surf Process Landforms* 44:1317-1329. <https://doi.org/10.1002/esp.4575>
- Wang JD, Li P, Gu Q, et al. (2019b) Changes in tensile strength and microstructure of loess due to vibration. *J Asian Earth Sci* 169:298-307. <https://doi.org/10.1016/j.jseae.2018.10.011>
- Wang JD, Xu YJ, Zhang DF, et al. (2021) Vibration-induced acceleration of infiltration in loess. *Sci China Earth Sci* 64:611-630. <https://doi.org/10.1007/s11430-020-9741-x>
- Wang JD, Zhang DF, Wang NQ, et al. (2019c) Mechanisms of wetting-induced loess slope failures. *Landslides* 16:937-953. <https://doi.org/10.1007/s10346-019-01144-4>
- Wu LZ, Zhang LM, Zhou Y, et al. (2017) Theoretical analysis and model test for rainfall-induced shallow landslides in the red-bed area of Sichuan. *Bull Eng Geol Environ* 77:1343-1353. <https://doi.org/10.1007/s10064-017-1126-0>
- Wu TY, Zhou CB, Jiang N, et al. (2020) Stability analysis for high-steep slope subjected to repeated blasting vibration. *Arab J Geosci* 13:828-840. <https://doi.org/10.1007/s12517-020-05857-y>
- Xie Q, Wu ZH, Dong J, Zhong S (2021) Matrix test measurements of ground-borne vibration induced by the heavy-duty trains on embankment and cutting tracks in a loess area. *Earthq Eng Vib* 20:605-620. <https://doi.org/10.1007/s11803-021-2041-8>
- Xu JB, Yan CG, Zhao X, et al. (2017) Monitoring of train-induced vibrations on rock slopes. *Int J Distrib Sens N* 13:1-7. <https://doi.org/10.1177/155014771668755>
- Xu JB, Li H, Du K, et al. (2018) Field investigation of force and displacement within a strata slope using a real-time remote monitoring system. *Environ Earth Sci* 77:552-563. <https://doi.org/10.1007/s12665-018-7729-3>
- Xu JW, Ueda K, Uzuoka R (2022) Evaluation of failure of slopes with shaking-induced cracks in response to rainfall. *Landslides* 19:119-136. <https://doi.org/10.1007/s10346-021-01734-1>
- Xue JY, Zhao XB, Zhang FL, et al. (2020) Shaking table tests on seismic behavior of the underground loess cave of earth building of traditional dwellings. *Eng Struct* 207. <https://doi.org/10.1016/j.engstruct.2020.110221>
- Yan WJ, Zheng HZ, Wu ZJ, et al. (2020) Experimental study and numerical analysis on the vibration characteristics of a terraced slope along an embankment section of a high-speed railway. *Shock Vib* 2020:1-14. <https://doi.org/10.1155/2020/4529842>
- Yang XT, Zhou YG, Cao Y, et al. (2023) On the determination of cyclic shear stress for soil liquefaction triggering in centrifuge model test. *Soil Dyn Earthq Eng* 173:108137. <https://doi.org/10.1016/j.soildyn.2023.108137>
- Yang ZP, Tian X, Jiang TW, et al. (2020) Experimental study on dynamic characteristics and dynamic responses of accumulation slopes under frequent microseisms. *Arab J Geosci* 13:770-781. <https://doi.org/10.1007/s12517-020-05781-1>
- Zhan XL, Liang J (2020) Analysis on the cause of a railway loess landslide and study on its treatment scheme. *Sub Eng* 6:190-196. (In Chinese)
- Zhang DF, Wang JD, Chen CL (2020a) Gas and liquid permeability in the variably saturated compacted loess used as an earthen final cover material in landfills. *Waste Manage* 105:49-60. <https://doi.org/10.1016/j.wasman.2020.01.030>
- Zhang DF, Wang JD, Chen CL, et al. (2020b) The compression and collapse behaviour of intact loess in suction-monitored triaxial apparatus. *Acta Geotech* 15:529-548. <https://doi.org/10.1007/s11440-019-00829-3>
- Zhang LL, Zhang J, Xu Y, et al. (2011) Reliability theory of geotechnical engineering. ShangHai: Tongji University Press. pp 1-168.
- Zhou Z, Shen JH, Tang S, et al. (2021) Analysis of weakening law and stability of sliding zone soil in thrust-load-induced accumulation landslides triggered by rainfall infiltration. *Water* 13:466-285. <https://doi.org/10.3390/w13040466>